Measurements of non-volatile aerosols with a VTDMA and their correlations with carbonaceous aerosols in Guangzhou, China

H. H. Y. Cheung[1], H. B. Tan[2], H. B. Xu[3], F. Li[2], C. Wu[1], J. Z. Yu[1,4] and C. K. Chan[1,5,6]

[1]{Division of Environment, Hong Kong University of Science and Technology, Hong Kong, China}

[2]{Institute of Tropical and Marine Meteorology, China Meteorological Administration, Guangzhou, China}

[3]{Sun Yat-sen University, Guangzhou, China}

[4]{Department of Chemistry, Hong Kong University of Science and Technology, Hong Kong, China}

[5]{Department of Chemical and Biomolecular Engineering, Hong Kong University of Science and Technology, Hong Kong, China}

[6]{School of Energy and Environment, City University of Hong Kong, Hong Kong, China}

Correspondence to: H. B. Tan (hbtan@grmc.gov.cn), C. K. Chan (chak.k.chan@cityu.edu.hk)

Abstract

Simultaneous measurements of aerosol volatility and carbonaceous matters were conducted at a suburban site in Guangzhou, China in February and March 2014 using a volatility tandem differential mobility analyzer (VTDMA) and an organic carbon/ elemental carbon (OC/EC) analyzer. Low volatility (LV) particles, with a volatility shrink factor (VSF) at 300°C exceeding 0.9, contributed to 5% of number concentrations of the 40 nm particles and 11–15% of the 80–300 nm particles. They were composed of non-volatile material externally mixed with volatile material, and therefore did not evaporate significantly at 300°C. Non-volatile material mixed internally with the volatile material were referred to as medium volatility (MV, $0.4 < VSF < 0.9$) and high volatility (HV, $VSF < 0.4$) particles. The MV and HV particles contributed to 57–71% of number concentration for the particles between 40 nm and 300 nm in size. The average EC and OC concentrations measured by the OC/EC analyzer were 3.4 ± 3.0 μg m^{-3} and 9.0 ± 6.0 μg m^{-3}, respectively. Non-volatile OC evaporating at 475°C or above, together with EC, contributed to 67% of the total carbon mass. In spite of the daily maximum and minimum, the diurnal variations in the volume fractions of the volatile material, HV, MV and LV residuals were less than 15% for the 80–300 nm particles. Back trajectory analysis also suggests that over 90% of the air masses influencing the sampling site were well-aged as they were transported at low altitudes (below 1500 m) for over 40 h before arrival. Further comparison with the diurnal variations in the mass fractions of EC and the non-volatile OC in $PM_{2.5}$ suggests that the non-volatile residuals may be related to both EC and non-volatile OC in the afternoon, during which the concentration of aged organics increased. A closure analysis of the total mass of LV and MV residuals and the mass of EC or the sum of EC and non-volatile OC was conducted. It suggests that non-volatile OC, in addition to EC, was one of the components of the non-volatile residuals measured by the VTDMA in this study.

1 Introduction

Carbonaceous aerosols comprising organic carbon (OC) and elemental carbon (EC) or black carbon (BC) are one of the major light absorption constituents and are abundant in particulate matter (PM) (Rosen et al., 1978; Hansen et al., 1984; Japar et al., 1986; Chow et al., 1993; Horvath, 1993; Liousse et al., 1993; Fuller et al., 1999; Putaud et al., 2010; Tao et al., 2014; Zhang et al., 2015). In China, the worsening of visibility degradation associated with PM is of increasing concern in recent years. In particular, numerous studies on air pollution were carried out in different cities in China including the Pearl River Delta (PRD) region which is a fast-developing economic zone (Cheng et al., 2006; Wu et al., 2007; Andreae et al., 2008; Chan and Yao, 2008; Gnauk et al., 2008; Tan et al., 2013a). In 2007, the mass concentrations of EC and OC measured at an urban Guangzhou (GZ) site were reported to vary from 6.8 to 9.4 µg m^{-3} and from 13.4 to 22.5 µg m^{-3} respectively (Yu et al., 2010).

Soot particles are often characterized in terms of EC and BC, depending on whether they are measured thermally or optically (Penner and Novakov, 1996; Lavanchy et al., 1999; Cheng et al., 2011 and references therein). Their optical properties are distinct when they are freshly produced (Novakov et al., 2003). After aging processes such as cloud processing, chemical reactions and coagulation, their structure, shape, size, mixing state and thus optical properties change (Horvath, 1993; Liousse et al., 1993; Ghazi and Olfert, 2012). EC is typically measured by thermal method such as the OC/EC analyzer (Chow et al., 2007), whereas BC is optically measured using instruments such as aethalometer (Hansen et al., 1984), multi-angle absorption photometer (Petzold and Schönlinner, 2004) and particle soot absorption photometer (Virkkula et al., 2005). However, it is not possible to retrieve the mixing state of soot particles with these techniques. To determine the mixing state of soot particles, single particle soot photometer (Stephens et al., 2003), soot particle aerosol mass spectrometer (Onasch et al., 2012) and Volatility Tandem Differential Mobility Analyzer (VTDMA) (Philippin et al., 2004) have been used.

Ambient aerosols have varying volatility properties based on their chemical compositions. VTDMA was first introduced by Rader and McMurry (1986) to study the behavior of aerosols upon thermal treatment. A volatility shrink factor (*VSF*) is defined as the ratio of the particle size after exposed to elevated temperature to the original particle size. Later Philippin et al. (2004) developed a VTDMA which was capable of evaporating volatile material in aerosols at temperatures up to 300°C. Non-volatile compounds at 300°C, such as EC, non-volatile organics and sea salt, can internally mix with (or be coated with) volatile material. Note that the terms "volatile" and "non-volatile" are here defined based on the operational parameters and how the aerosol behave, when heated to 300°C in the VTDMA. They are different from the volatilities defined under ambient conditions (Donahue et al., 2009; Murphy et al., 2014) or in other measurement techniques (Twomey, 1968; Pinnick et al., 1987; Huffman et al., 2009). The composition of these non-volatile residuals can vary spatially and temporally. Previous studies have demonstrated a good agreement between the mass concentration of BC and the mass concentration of non-volatile particles that experienced size reductions of 5 to 10% upon heating at 300°C in the VTDMA (Frey et al., 2008). Various studies have also used the VTDMA to estimate the mixing states of soot particles (Philippin et al., 2004; Rose et al., 2011; Levy et al., 2014; Zhang et al., 2016). Particles with small volatile fractions, i.e. $VSF > 0.9$ at 300°C, are often assumed to be soot particles externally mixed with particles with volatile material at 300°C. Particles with larger volatile fractions, i.e. $VSF < 0.9$ at 300°C, were assumed to represent soot particles internally mixed (coated) with the volatile material (Cheng et al., 2006; Wehner et al., 2009).

Organics also contribute to light absorption by atmospheric particles (Bond, 2001; Kirchstetter et al., 2004; Chen and Bond, 2010). Laboratory studies have shown that organic aerosols may form low volatility oligomers after aging for a long time (e.g. Kalberer et al., 2004). Huffman et al. (2009) showed that highly oxygenated, aged organic aerosols exhibited similar or lower volatility than the primary organic aerosols or the less oxygenated particles. Recently, Häkkinen et al. (2012) compared the residual mass derived from a volatility differential mobility particle sizer (VDMPS) at 280°C with BC measured by an aethalometer and organics measured by an Aerodyne aerosol mass spectrometer (AMS). It was found that the mass fraction remaining of non-BC residuals in VDMPS measurements was positively correlated with the mass fraction of organics in AMS measurements.

In this study, simultaneous measurements of aerosols volatility and carbonaceous matter were made at a suburban site in Guangzhou, China during wintertime in February and March 2014 using a VTDMA and a semi-continuous OC/EC analyzer, respectively. The volatility measurements were made for ambient aerosols ranging from 40 nm to 300 nm in diameter. Here residuals remaining after heating at 300°C in the VTDMA are referred to as non-volatile in this study. We report the average values, time series and diurnal variations in the number and volume fractions of the volatile and non-volatile material, as well as the OC and EC concentrations. We examine the relationships of the non-volatile material upon heating at 300°C to EC and to the non-volatile OC, based on analyses of the diurnal patterns and mass closures of the OC/EC and VTDMA data. Finally, we discuss the influence of air mass origins on the volatility of the sampled aerosols and concentrations of OC and EC based on back trajectory analysis.

2 Methodology

2.1 Experimental

2.1.1 Measurement details

The campaign took place at the China Meteorological Administration (CMA) Atmospheric Watch Network (CAWNET) Station in Panyu, Guangzhou, China in summer from July to September 2013 and in winter from February to March 2014. The station is operated by the Institute of Tropical and Marine Meteorology (ITMM) of the CMA. The Panyu station is located at the center of the PRD region and on the top of Dazhengang Mountain (23°00’ N, 113 °21’ E) with an altitude of about 150 m (Fig. S1 in Supplemental Information) (Tan et al., 2013a). It is about 120 m above the city and is surrounded by residential neighborhoods with no significant industrial pollution sources nearby. Measurements of particle number size distributions, volatility, mass concentrations of EC and OC in winter were made from 6 February to 21 March 2014. Some of the measurements were not made continuously due to maintenance work and hence only the periods with concurrent VTDMA and OC/EC measurements were analyzed.

2.1.2 VTDMA measurements

We used a custom-made VTDMA based on a Hygroscopic TDMA system developed in ITMM (Tan et al., 2013b), with the humidifier between the two DMAs replaced by a heated tube which induce evaporation of volatile material. In our VTDMA system shown in Fig. 1, ambient aerosols were sampled by a $PM_{2.5}$ inlet and subsequently passed through a dryer at relative humidity below 20%. The dry aerosols were then directed through a neutralizer and entered the first differential mobility analyzer (DMA_1) (Stream 1) to produce mono-disperse aerosols of diameter between 40 nm and 300 nm, D_0. The mono-disperse aerosols went either via path (a) or (b) in Fig. 1 after leaving the DMA_1. In path (a), they (Stream 2) were directed to a condensation particle counter (CPC, TSI Model 3772) to obtain particle counts, N_{D0}. The particle number size distribution of the ambient aerosols, $dN/dlogD_p$, was also measured by varying the DMA_1 voltage (SMPS scan). Afterwards, the mono-disperse aerosols were directed via path (b) to a heated tube for volatility measurement (V-Mode) sequentially at 25°C, 100°C and 300°C. The heating tube was a 1/2'', 80 cm long stainless steel tube with an inner diameter of 8 mm. With a sample flow rate of 1 L min^{-1}, the resulting residence time in the heated section of the VTDMA was 2.4 s. The estimated aerosol velocity on the center line was 0.33 m s^{-1}. Compared to the residence time of 0.3 s to 1 s in other VTDMA systems (e.g. Brooks et al., 2002; Philippin et al., 2004; Villani et al., 2007), the residence time in our VTDMA is assumed to be long enough for the volatile material to be effectively vaporized. After leaving the heating tube, the flow entered a heat exchanger measuring 30 cm in length to ensure sufficient cooling before entering DMA_2.

Upon heating, volatile components of particles such as sulfate, nitrate and volatile organics vaporize at different temperatures depending on their volatilities. As mentioned in Section 1, the volatility shrink factor, *VSF*, is defined as the ratio of particle diameter after heating at temperature T, $D_{p,T}$, to the diameter before heating, D_0:

$$VSF(T) = \frac{D_{p,T}}{D_0} \tag{1}$$

The *VSF* indicates the size reduction of the ambient particles upon heating. The value of *VSF* is always smaller than or equal to one, depending on the amount of volatile material vaporized at the heating temperature T. The *VSF* is used to divide the particles into three groups, namely low volatility (LV), medium volatility (MV) and high volatility (HV) particles. In this study, we focus on the measurements made at 300°C. The *VSF* ranges for the LV, MV and HV particles upon heating at 300°C are defined as follows: above 0.9, between 0.4 and 0.9 and below 0.4, respectively (Fig. 2) (Wehner et al., 2004; Wehner et al., 2009).

The size distribution, $dN'/dlogD_p$ of the remaining particles (hereafter the residuals) were measured by DMA_2 and CPC (Fig. 2b). It can provide information of the mixing state of the sampled aerosols. A uni-modal distribution indicates the presence of internally-mixed particles exhibiting uniform size reduction upon heating, whereas a multi-modal distribution indicates externally-mixed particles of different composition and volatilities. In the multi-modal distribution, each mode represents particles of similar composition and volatility. In this study, multiple modes of LV, MV and HV were observed in the distribution after heating. The LV particles were assumed to represent EC and non-volatile OC externally mixed with the volatile material, while MV and HV particles were assumed to represent EC and non-volatile OC internally mixed with volatile material. While the volatile material in the MV and HV particles were referred to as VM, those exist as external mixtures with the LV, MV and HV particles were referred to as completely vaporized (CV) particles. The CV particles evaporated completely without leaving behind any residuals at 300°C. Excluding particle diffusional and thermophoretic losses, and assuming that the residual material did not evaporate to the sizes below the detection limit of the CPC (here 10 nm), the evaporation of VM and CV did not change the number concentrations of LV, MV and HV particles.

Overall it took around one and a half to two hours to complete a cycle of measurements which consisted of SMPS scans and V-Mode measurements at 25°C, 100°C and 300°C. At each temperature, the sampling time for six selected diameters from DMA_1 (40 nm, 80 nm, 110 nm, 150 nm, 200 nm and 300 nm) took about half an hour and SMPS scans were made in-between. Hereafter, notations with the superscript prime refer to the LV, MV or HV residuals measured by DMA_2 and CPC after heating, while the corresponding ones without the prime refer to the LV, MV or HV residuals in ambient aerosols prior to heating.

2.1.3 OC/EC measurements

A semi-continuous Sunset OC/EC Analyzer (Model 4) was used to measure $PM_{2.5}$ mass concentrations of organic carbon and elemental carbon, m_{OC} and m_{EC} respectively, on an hourly basis (Turpin et al., 1990; Birch and Cary, 1996; Wu et al., 2012). With the OC/EC Analyzer the ACE-Asia protocol (a NIOSH-derived protocol) was adopted, in which OC was evaporated at four set temperatures of 310°C, 475°C, 615°C and 870°C with pure helium (He) as a carrier gas, whereas EC was combusted at temperatures between 550°C and 870°C under He and 2% oxygen (O_2) (Schauer et al., 2003; Wu et al., 2012). The OC contents were named OC_1 to OC_4 based on the temperature protocol of the OC/EC analyzer (Table 1). The mass of EC determined at different temperatures was grouped together in subsequent analysis.

It is plausible that in the VTDMA measurements, there were volatile or semi-volatile OC that vaporize at 300°C or below. This vaporized OC is assumed to correspond to $OC_{1,}$ which was vaporized at 310°C although this OC/EC temperature was slightly higher than the temperature of 300°C in the VTDMA. With this assumption, the residual particles of the VTDMA at 300°C (LV and MV residuals) are postulated to consist of (1) OC_2 to OC_4, which were vaporized at 475°C and above, and (2) EC and other refractory PM components. We have ignored the HV residuals as their contributions to the total volume of the particles were insignificant in comparison with LV and MV residuals (Section 3.1). In Section 3.5, we will conduct a mass closure analysis based on the VTDMA and OC/EC measurements to examine this assumption.

2.2 Data analysis

2.2.1 Number fractions

The number fractions of LV, MV and HV residuals ($\Phi'_{N,LV}$, $\Phi'_{N,MV}$ and $\Phi'_{N,HV}$, with their sum being equal to unity) in Stream 2 on Fig. 1 were obtained from $dN'/dlogD_p$ measured by the VTDMA. However, these fractions do not represent the actual number fractions of LV, MV and HV particles ($\Phi_{N,LV}$, $\Phi_{N,MV}$ and $\Phi_{N,HV}$) before heating because some of the particles can evaporate completely (CV) and due to diffusion and thermophoretic losses. The number fraction of CV ($\Phi_{N,CV}$) was first obtained by considering the number fractions of the residuals ($1-\Phi_{N,CV}$) and the number concentrations at a selected diameter D_0 before heating (N_{D0}) and after heating (N'):

$$N_{D_0} \cdot \eta_{D_0} \cdot \left(1 - \Phi_{N,CV}\right) = N' \tag{2}$$

where η_{D0} is the transport efficiency of particles.

In Eq. (2) we assume that η is the same for LV, MV and HV particles. η accounts for particle losses between DMA_1 and DMA_2 due to diffusion and thermophoretic forces (Philippin et al., 2004), and it varies as a function of particle size and heating temperature. η at each particle diameter and VTDMA temperature was determined in laboratory calibrations with sodium chloride (NaCl) particles, which do not evaporate (i.e., $\Phi_{N,CV} = 0$) at the temperatures used in our experiments. The transmission efficiency of NaCl of several selected diameters in temperatures between 50°C and 300°C is provided in the supplemental information (Fig. S2). From the known η and observational data obtained with the VTDMA providing N_{D0} and N', $\Phi_{N,CV}$ can be calculated from Eq. (2). Afterwards, $\Phi_{N,LV}$, $\Phi_{N,MV}$ and $\Phi_{N,HV}$ were obtained by renormalizing $\Phi'_{N,LV}$, $\Phi'_{N,MV}$ and $\Phi'_{N,HV}$ with ($1-\Phi_{N,CV}$) so that the sum of $\Phi_{N,LV}$, $\Phi_{N,MV}$, $\Phi_{N,HV}$ and $\Phi_{N,CV}$ equaled unity.

2.2.2 Volume fractions

The volume fractions of LV, MV, HV residuals and CV ($\Phi_{V,LV}$, $\Phi_{V,MV}$, $\Phi_{V,HV}$ and $\Phi_{V,CV}$) at each selected diameter D_0 are defined as the ratios of the volume of LV, MV, HV residuals and CV to the total volume of the mono-disperse particles before heating. By assuming that the residuals are spherical in shape, $\Phi_{V,LV}$, $\Phi_{V,MV}$ and $\Phi_{V,HV}$ can be calculated by:

$$\Phi_{V,i} = \frac{N_i \times \frac{\pi}{6} D_{p,i}^3}{N_{D_0} \times \frac{\pi}{6} D_0^3} = \Phi_{N,i} \cdot \frac{D_{p,i}^3}{D_0^3} \tag{3}$$

where N_i and $D_{p,i}$ are the number concentration and mean residual diameter of i = LV, MV or HV residuals.

For LV particles, it is assumed that D_0 and mean D_p are the same and hence $\Phi_{V,LV}$ is the same as $\Phi_{N,LV}$. For MV and HV particles, the mean D_p is smaller than D_0 due to the evaporation of volatile material. The number weighted mean residual diameter (D_p) was calculated by:

$$D_{p,i} = \frac{\sum_j D_{p,i} \cdot N_{i,j}}{N_i} \tag{4}$$

where $D_{p,i}$ and $N_{i,j}$ are the residual diameter and number concentration of i = MV or HV at the 75 diameter bins (j) of *VSF*, respectively.

The volume fractions of the evaporated material were calculated from the volume fractions of the residuals. The calculation for $\Phi_{V,CV}$ was similar to that for $\Phi_{V,LV}$. Since the particle has completely vaporized, the vaporized volume is equivalent to the volume of the original particle. Hence, $\Phi_{V,CV}$ is the same as $\Phi_{N,CV}$:

$$\Phi_{V,CV} = \frac{N_{\mathrm{CV}} \cdot \frac{\pi}{6} D_{p,\mathrm{CV}}^3}{N_{Do} \cdot \frac{\pi}{6} D_o^3} = \Phi_{N,CV} \tag{5}$$

where $D_{p,\mathrm{CV}} = D_0$. Since the sum of the total volume fraction of CV, VM and the residuals of LV, MV, HV equaled unity, $\Phi_{V,VM}$ was obtained after the above volume fractions were calculated. Furthermore, we also calculated the volume fraction remaining (*VFR*), defined as the volume ratio of the residual to its host particle, to aid our discussions later:

$$VFR_i = \frac{N_i \cdot \frac{\pi}{6} D_{p,i}^3}{N_i \cdot \frac{\pi}{6} D_0^3} = \frac{D_{p,i}^3}{D_0^3} \tag{6}$$

where N_i and $D_{p,i}$ are the number concentration and mean residual diameter of i = MV or HV after heating, respectively.

2.2.3 Particle size distributions of number, volume and mass concentrations of LV, MV and HV residuals

Due to the differences in the size cuts of the VTDMA and the OC/EC analyzer, log-normal fits extrapolated to 5 µm were applied to the particle number size distributions of the residuals of LV, MV and HV ($dN/dlogD_{p,i}$, where i = LV, MV or HV) to estimate the volume and then mass concentrations of the ambient aerosols for comparison with $PM_{2.5}$ OC/EC measurements. The volume size distributions ($dV/dlogD_{p,i}$) were calculated by:

$$\frac{dV}{dlogD_{p_i}} = \frac{dN}{dlogD_{p_i}} \cdot \frac{\pi}{6} D_{p,i}^3 \tag{7}$$

where $D_{p,i}$ is the mean residual diameter as defined in Section 2.2.2.

Volume (V) concentrations of LV, MV and HV residuals can then be calculated by integrating the area under the fitted curves. As we only focus on LV and MV, densities of 1.0 g cm^{-3} (Hitzenberger et al., 1999) and 1.5 g cm^{-3} are applied to V_{LV} and V_{MV} to obtain mass (m) concentrations of LV and MV residuals, respectively. The choice of the densities is based on the assumption that LV and MV residuals are dominated by soot and non-volatile OC, respectively.

3 Results and Discussions

3.1 Overview

The time series of meteorological conditions, particle number size distribution, $PM_{2.5}$, OC and EC concentrations during the campaign are presented in Fig. 3. Overall, the campaign was under the influence of the prevailing northerly wind with an average wind speed and temperature (± one standard deviation) of 1.73 ± 0.95 m s^{-1} and 14.8 ± 5.1°C, respectively. The average $PM_{2.5}$ concentration was 48 ± 26 µg m^{-3}. A few colder periods were observed, during which the wind speed increased and the temperature decreased. In general, the low wind speed favored the accumulation of $PM_{2.5}$. During the campaign OC concentrations ranged from 0.5 to 47.0 µg m^{-3} with an average of 9.0 ± 6.0 µg m^{-3}, while EC concentrations ranged from 0.2 to 23.0 µg m^{-3} with an average of 3.4 ± 3.0 µg m^{-3}. OC_1, the most volatile group among OC_1 to OC_4 in OC/EC analysis, accounted for one-third of the total carbon mass (Fig. 4).

On 17 Feb, 12 and 17 Mar 2014, the daily-averaged $PM_{2.5}$ concentrations exceeded 95 μg m^{-3}; and they were nearly twice the daily-averaged values of the other days (Fig. 3, shaded area in grey). Results of 72 h back trajectories (Stein et al., 2015; Rolph, 2016) showed that air masses arriving at the site on or before these three days mostly originated from the continental or oceanic area close to Eastern China (Fig. S3). The SMPS data also showed a mode near 100 nm with a high particle number concentration (Fig. 3).

The temporal variation of the number concentration of MV particles having an initial diameter of 80 nm or above tracked reasonably well with the accumulation of $PM_{2.5}$ as the particles aged and became more internally mixed (Fig. 3 and S4). Furthermore, the number concentration of MV particlces showed a size dependence in the 80–300 nm particles. There were days, e.g., from 24 Feb to 10 Mar 2014, when the number concentration of 300 nm MV particles did not track well with $PM_{2.5}$ mass concentration. The mode of the total particle number size distribution was below 100 nm and the number concentrations of 300 nm particles were low (Fig. 3). $PM_{2.5}$ mass concentration tracked better the number concentrations of 80 nm to 150 nm MV particles (Fig. 4a to S4c) than those of 200 nm and 300 nm MV particles (Fig. S4d and S4e).

The average number and volume fractions of CV, HV, MV and LV in VTDMA measurements at 300°C are summarized in Table 2. VM is internally mixed with MV and HV residuals, and hence does not have a separate contribution to number concentrations. Overall, HV and MV particles, indicator for aged aerosols with internally mixed non-volatile and volatile material, accounted for 57% to 71% of the total particle number concentration. Non-volatile material (LV, MV and HV residuals) accounted for 15% to 26% of the total volume of selected particles before heating. While the CV and HV fractions were larger in the finest particles selected (D_0 = 40 nm), MV and LV were more abundant in larger particles (D_0 > 80 nm). As in Rose et al. (2006), fresh emissions like soot adsorb or absorb volatile material during atmospheric processing. The smaller particles grew faster than the larger ones because of their higher ratio of surface area to volume. When they were heated in the VTDMA at 300°C, the smaller particles reduced more substantially in size, as reflected in the higher CV and HV fractions and lower MV and LV fractions. The higher abundance of MV and LV in the larger size particles could also be explained by the aged particles arriving at the sampling site. Since the sampling site is located on top of a mountain with an altitude of 150 m, the particles were likely aged upon arrival. Non-volatile particles in the ultrafine modes from fresh emissions can be aged with both non-volatile and volatile material, and became larger in size. Nevertheless, the detection limit of the downstream DMA and CPC in the VTDMA system is 10 nm. The particles with diameters below the detection limit leads to an overestimation of CV and an underestimation of the non-volatile residuals for the finest particles selected (with an initial diameter of 40 nm).

3.2 Diurnal variations

Figure 5 shows diurnal variation in the fraction of CV, HV residual, MV residual, LV residual and VM in the total volume of particles of dry initial diameters of 40, 150 and 300 nm. For 40 nm particles, a clear maximum and minimum of the fraction of CV, VM and HV residuals are observed at 08:00 and 13:00, respectively. The diurnal variation of the HV and MV particles in the 40 nm particles was clearer in terms of number fraction (Fig. S5). Furthermore, the trend of CV was opposite to those of VM, HV and MV. The increase of CV in the 40 nm particles and to a lesser extent of LV in the 150 nm and 300 nm particles in the morning is consistent with traffic pattern. Fresh emissions of volatile and non-volatile material, likely OC and EC, were externally mixed and contributed to CV and LV, respectively. As time progresses in a day, the highly volatile species (CV) which were freshly emitted in the morning, may evaporate and react to form less volatile particles and become VM instead of CV (Robinson et al., 2007). Alternatively, these CV particles could also coagulate with smaller particles to form VM containing particles. Less fresh emissions with more CV particles turning into VM on MV and HV particles could explain the trend that the number and volume fractions of CV decreased while those of MV and HV increased (Fig. 5 and Fig. S5).

We also used the diurnal variations in the volume fraction remaining (*VFR*), again defined as the volume ratio of the residual to its *host* particle (not to the total volume of all particles), to examine the size changes of the non-volatile residuals of HV and MV particles. The *VFR* of HV did not exhibit any obvious diurnal variations but the *VFR* of MV peaked near 18:00. The *VFR* of the 40 nm MV particles increased after 14:00 while those of the 150 nm and 300 nm MV particles increased after 15:00. Since the *VFR* of HV and MV were relatively constant during the day, the increase in the VM fraction after the morning rush hours could be attributed to the increase in the number concentrations of the HV and MV particles instead of changes in the amount of VM on the MV or HV residuals.

The diurnal variations for particles larger than 80 nm were much less obvious than those for 40 nm particles in this study and in others (Rose et al., 2011; Cheng et al., 2012; Zhang et al., 2016). In winter, the atmosphere is more stable, resulting in a poorer dilution of aged particles with the less polluted aerosols from higher up (Rose et al., 2006). When the aged pollutants were trapped near the ground, the effect of aging of fresh emissions weakened. Therefore, although a daily maximum and a daily minimum were still observed for particles larger than 80 nm, the variation was mostly within 15%.

The diurnal variations in the mass fractions of OC and EC in $PM_{2.5}$ provided further insights to the observations above (Fig. 6). The OC and EC data on Mar 12 and 17 were excluded since they were more than two standard deviations higher than those on other days. Subtle morning peaks between 06:00 and 10:00 were observed for the volume fraction of LV residuals (Fig. 5). A similar peak was observed for the mass fraction of EC in $PM_{2.5}$ in the morning (Fig. 6). This suggests that the LV particles may be related to the EC from vehicle emissions in the morning. This EC was relatively less aged and externally mixed with the other volatile material. In the late afternoon, the LV residuals showed another peak between 17:00 and 19:00 whereas the mass fraction of EC in $PM_{2.5}$ exhibited a minimum at 15:00, after which it increased continuously. The continuous increase in EC at night is likely related to the increase of heavy-duty diesel traffic (Zhang et al., 2015), which was restricted during daytime (Bradsher, 2007).

Although OC_1 contributed to about half of the total OC mass, the diurnal variation in the mass fraction of OC in $PM_{2.5}$ was driven by the total mass of OC_2, OC_3 and OC_4 (OC_{2-4}), which reached a minimum between 05:00 and 09:00 and increased until 19:00. OC can be attributed to both primary and secondary sources. The increased mass fraction of OC in $PM_{2.5}$ and OC-to-EC ratio in the afternoon suggest that the sources of OC were less related to traffic but more to the aging and formation of secondary organic aerosols (Turpin et al., 1990; Chow et al., 1996). These OC_2, OC_3 and OC_4 may be highly oxygenated species or oligomers that are less volatile than primary or less oxygenated organics (Kalberer et al., 2004; Huffman et al., 2009).

It is interesting to note that the volume fraction of the LV residuals and the *VFR* of MV particles at different sizes showed a dip in the afternoon (Fig. 5, third column from the left). The *VFR* of 40 nm MV particles showed a dip at 14:00 while those in 150 nm and 300 nm particles showed a dip at 15:00. The volume fraction of LV residuals in 150 nm and 300 nm particles reached a minimum at 13:00 and 15:00, respectively. Because EC decreased between 12:00 and 15:00, the increase in the volume fraction of LV residuals in 150 nm particles since 13:00 and the *VFR* of 40 nm MV particles since 14:00 may be related to the increased presence of aged organics as well as the EC particles which aged via coagulation and condensation.

3.3 Back trajectory analyses

We calculated 72 h back trajectories of air masses arriving at the sampling site (23°00 N, 113°25’’ E) at 4 h intervals (at 00:00, 04:00, 08:00, 12:00, 16:00 and 20:00 local time, UTC +8) using the PC version of the HYSPLIT4 (Hybrid Single Particle Lagrangian Integrated Trajectory, version 4) model (Stein et al., 2015; Rolph, 2016). Archived meteorological data from the Global Data Assimilation System (GDAS) 1-deg was employed and the receptor height was set at 500 m above ground level (a.g.l.). The 191 back trajectories calculated were grouped into six clusters based on their spatial distribution (Fig. 7).

Overall, the sampling site was mostly affected by northwesterly and northeasterly air masses. Clusters 1 and 3 are coastal and continental air masses, respectively, although both originated from the northeast. Clusters 4, 5 and 6 represent continental air masses originating from the northwest. Cluster 2 is a group of maritime air masses originating from the East China Sea northeast or east of Guangzhou. While the air masses in cluster 6 were transported at relatively high speeds and altitudes (over 3000 m a.g.l.), the air masses in all the other clusters were transported at an altitude below 1500 m a.g.l. for over 40 h before arriving at the site. As the air masses in cluster 6 only occurred for less than three days and since the corresponding VTDMA and OC/EC data were sometimes unavailable, cluster 6 will be excluded from the following discussion.

The average $PM_{2.5}$, OC and EC concentrations associated with the air masses from the northeast of Guangzhou (clusters 1, 2 and 3) were higher than those from the northwest (clusters 4 and 5, Table 3). Days associated with the coastal and maritime air masses were more polluted than days associated with continental air masses for several reasons. First, south China as a region is often affected by the high pressure system moving eastward or southward from the continent out to sea in winter. When the maritime or coastal air streams entered from the southeast of the sampling site at Panyu, the atmosphere at the sampling site became more stable with low local wind speeds (e.g. the polluted days on Feb 17 and Mar 12, 16 and 17, Fig. 3 and S3). The local pollutants accumulated and the city was also affected by pollutants from the southeastern areas of the site (e.g. Shenzhen, Nansha and Dongguan). Second, land-sea breeze circulation were observed when the sampling site was under the influence of maritime air masses from Mar 18 to 20. During the day, southeasterly wind prevailed and the wind speed was higher. In the evening, the southeasterly wind was gradually replaced by a southwesterly or northwesterly wind and the wind speed decreased (Fig. 3). The cycle started again in the morning when the westerly wind was gradually replaced by southeasterly wind. Such land-sea breeze effects can result in an effective redistribution and accumulation of air pollutants within the PRD region (Lo et al., 2006).

Furthermore, $PM_{2.5}$ in the northeastern parts of China can exceed 200 μg m^{-3} due to both enhanced emissions from coal combustion for heating and poor dispersion during wintertime (Gu et al., 2014). Under the influence of the prevailing northerly or northeasterly wind in China, these pollutants were often transported to southern China and the East China Sea (Chen et al., 2012). The pollutants might also have accumulated when the maritime air masses spent about two days across Taiwan and the coast of south China. In contrast, continental air masses in cluster 5 moved slightly faster, and were often associated with the cold front period during which the local wind speed and pressure increased but the temperature decreased (Fig. 3). As the cold air masses passed through the city, dispersion and clearance of pollutants were promoted, resulting in lower $PM_{2.5}$ concentrations (Tan et al., 2013a). Therefore, unlike in other coastal cities like Hong Kong (Lee et al., 2013), in Panyu the maritime air masses could lead to more severe pollution than the continental ones in winter.

The five clusters were further analyzed to study the influence of air mass history on aerosol volatility. The number fractions of CV, HV, MV and LV of the six selected diameters in VTDMA measurements are regrouped based on the clusters as shown in Fig. 8. The total number fractions of the non-volatile residuals (sum of HV, MV and LV) were similar in all clusters. The maritime air masses (cluster 2) had a slightly higher fraction of LV particles while the continental air masses originating from the northwest of the site (clusters 4 and 5) had a higher fraction of HV particles. Although the air masses in clusters 1 and 5 originated from further away and traveled at relatively higher speeds than those in clusters 2, 3 and 4, all the clusters involved transport at low altitudes (below 1500 m) for over 40 h, likely due to the generally lower mixing heights in winter. Therefore, it is plausible that the aerosol particles in these air masses were all well-aged upon arrival. Similar results were observed in Beijing by Wehner et al. (2009). This could be another reason for the lack of size dependence of the number, volume fractions and diurnal variation for the particles larger than 80 nm. When the transported air masses mixed with the local pollutants, the size dependence of the number fractions of different volatility groups as well as the aging of local emissions was further reduced.

We also examined the volatility shrink factor (*VSF*) distributions of 40 nm, 110 nm and 300 nm particles upon heating at 300°C (Fig. 9). Log-normal fittings with a three-peak solution were applied to the distributions. The average *VSF* modes of the peaks were located at 0.38 ± 0.021 (peak 1), 0.60 ± 0.066 (peak 2) and 0.95 ± 0.007 (peak 3), respectively. The standard deviation of the corresponding normal distribution (σ) of peak 3 was the smallest among the three peaks ($\sigma < 0.1$). For the same particle size, the *VSF* distributions in the *VSF* range between 0.3 and 0.8 in cluster 5 was relatively more uni-modal than those of other clusters (Fig. 9b and 9c). This suggests that the composition in cluster 5 was more homogeneous. Cluster 1 also consisted of long-range transported air masses but they likely passed through areas that are more polluted and mixed with different types of pollutants.

3.4 New particle formation

Two new particle formation (NPF) events were observed in the campaign on 20 Feb and 13 Mar 2014 (Fig. 3). Since VTDMA data were not available during the NPF event on 13 Mar 2014, we only focus on the NPF event on 20 Feb 2014 which happened after a cold front under a low PM2.5 concentration. On 20 Feb 2014, a sub-20 nm particle mode was first observed at 12:00. This particle mode grew continuously until it reached 120 nm at 02:00 on 21 Feb 2014. In the VTDMA data, a sharp increase in the number concentration of HV particles having an initial diameter of 40 nm was observed at 17:00 on 20 Feb 2014 (Fig. 10). This event is likely related to the growth of the newly formed particles when they mixed with the volatile material accumulated via condensation or adsorption. The volatile material which extensively condensed on the pre-existing particles could be sulfate, ammonium and organics. They were found to be the major species contributing to particle growth in the NPF events at different locations (Zhang et al., 2004; Smith et al., 2008; Zhang et al., 2011; Yue et al., 2016). Zhang et al. (2004) observed that sulfate was always the first and the fastest species to increase in concentration during an NPF event. They also suggested that photochemically formed secondary organics contributed significantly to the growth of the ultrafine particles. Recently, Yue et al. (2016) reported that sulfate, ammonium and organics were the main contributors to particle growth in the NPF events in Taoyuan of the PRD region. As these particles aged further, they grew larger as reflected in the increase in number concentrations of larger MV particles and the increase in $PM_{2.5}$ mass (Fig. 10). Similar results were also observed in the study in Beijing by Wehner et al. (2009). Furthermore, the growth of the newly formed particles can also be observed from the number size distributions of the HV, MV and LV particles at different times on 20 and 21 Feb 2014 (Fig. 11). The mode of the HV particles increased from 40 nm at 17:00 to 80 nm at 21:00 on 20 Feb 2014. The mode stayed at 80 nm while the corresponding number concentration decreased at 02:00 on 21 Feb 2014. In contrast, the number concentration and diameter mode of the MV particles grew continuously. The HV and MV particle concentrations and diameter modes underwent much smaller changes on the non-event day of 28 Feb 2014 (Fig. 11).

3.5 Closure analysis for LV and MV residuals at 300°C, OC and EC

The closure analysis of EC or the sum of EC, OC_2, OC_3, and OC_4 and the total mass of LV and MV residuals was conducted (Fig. 12). Good correlations ($R^2 > 0.9$) for both EC and the sum of EC, OC_2, OC_3, and OC_4 with the total mass of LV and MV residuals were obtained. Nonetheless, the slope for the total mass of LV and MV residuals to the mass of EC (2.94) is more than two times of that for the total mass of LV and MV residuals to the sum of EC, OC_2, OC_3, and OC_4 (1.22), indicating that EC alone cannot account for the total mass of LV and MV residuals. Including non-volatile OC (sum of OC_2 to OC_4) gave a better mass closure with the total of LV and MV residuals. This further supports our initial postulation that the non-volatile residuals which remained intact upon heating at 300°C in the VTDMA may contain a significant amount of non-volatile OC. However, the total mass of EC, OC_2, OC_3, and OC_4 did not explain all the mass of LV and MV residuals. A possible explanation could be that the vaporizing temperatures of some OC_1 are close to the upper limit (310°C), hence they were not completely vaporized in the heated tube and remained in the non-volatile residuals. The presence of other refractory material and the assumption made about the density of LV and MV are two other possible explanations.

Other possible errors for the closure could be related to the different heating environments in the VTDMA and the OC/EC analyzer. In the OC/EC analyzer, OC was measured when the samples were heated in the presence of a non-oxidative carrier gas (He). In the VTDMA, aerosols were heated in air which contained O_2. Therefore, some "$OC_{2\text{-}4}$" that evaporated at 475°C or above in the OC/EC analyzer may have been oxidized at 300°C in the VTDMA. Charring of organic matter could also occur (Philippin et al., 2004). Further study is needed to quantify the effect of oxygen on the oxidation of OC in the VTDMA. The extrapolated lognormal fitting of the size distribution of non-volatile particles can also cause errors if the mode diameter of the fitting is beyond the VTDMA's range of measurements. While the VTDMA measured the size distribution of particles between 10 nm and 400 nm in diameter, the OC/EC analyzer took into account particles up to 2.5 µm in diameter. Yu et al. (2010) reported three EC and OC modes between 400 nm and 10 µm in ambient aerosols in Guangzhou: 400 nm, 900 nm and 5 µm. The 400 nm mode accounted for 44% to 49% of the measured EC but only 17% to 20% of the measured OC.

4 Conclusions

This study presents the first VTDMA measurements in a suburban area of Guangzhou in the Pearl River Delta region, China during wintertime. The non-volatile material at 300°C in VTDMA measurements was assumed to be EC and non-volatile OC. The LV particles, representing non-volatile material externally mixed with the volatile material,, contributed to less than 20% of the total particle number concentration at the sampling site. The diurnal variations in the number and volume fractions of LV, MV and HV were much less obvious in this study than in other studies (e.g. Rose et al., 2011; Cheng et al., 2012; Zhang et al., 2016) likely because of the more stable atmosphere and poorer dilution of aged aerosols in winter. The back trajectory analyses showed that the measured $PM_{2.5}$, EC and OC concentrations were higher when the sampling site came under the influence of maritime and coastal air masses originating from the east or northeast of the site. These observations were attributed to the high pressure system on continent, the prevailing northerly wind and the enhanced pollution from north China in winter. The long-range transport continental trajectories were often associated with the cold front periods during which the dispersion of pollutants was promoted. The number fractions of LV, MV and HV particles did not show much variations among the trajectory clusters, likely because the air masses in all the clusters were transported at low altitudes (below 1500 m) for over 40 h. They were therefore well-aged upon arrival at the site.

While previous studies have indicated soot as a major component of the non-volatile residuals at 300°C measured by the VTDMA (e.g. Philippin et al., 2004; Frey et al., 2008), Häkkinen et al. (2012) and this work identified non-volatile organics as another possible component. The diurnal variations in the LV fractions and the size of the MV residuals may be related to the variation in the abundance of both EC and non-volatile OC, which evaporated at 475°C and above in the OC/EC analyzer. The analyses of the diurnal variations in the LV fractions and the *VFR* of MV particles, the latter of which reflects the change in size of the non-volatile material in the MV particles, suggest that the increase in the non-volatile fractions and in the size in the early afternoon may be related to the increase in non-volatile OC in addition to the effects of coagulation and condensation. The mass closure analysis of EC and the total mass of LV and MV residuals also indicated that EC alone cannot account for the mass of the non-volatile residuals. The total mass of EC and and non-volatile OC gave a better closure with the total mass of the LV and MV residuals, suggesting that the non-volatile OC may have contributed to the non-volatile residuals in our VTDMA measurements.

Acknowledgements

This work is supported by the Research Grants Council of the Hong Kong Special Administrative Region, China (Project No. 600413), the Natural Science Foundation of China (Grant 41375156), Special Research and Development Fund for Research Institutes (2014EG137243) and the National Key Project of Basic Research (2011CB403403).

References

Andreae, M. O., Schmid, O., Yang, H., Chand, D., Zhen Yu, J., Zeng, L.-M., and Zhang, Y.-H.: Optical properties and chemical composition of the atmospheric aerosol in urban Guangzhou, China, Atmos. Environ., 42, 6335-6350, 2008.

Birch, M. E. and Cary, R. A.: Elemental carbon-based method for monitoring occupational exposures to particulate diesel exhaust, Aerosol Sci. Technol., 25, 221-241, 1996.

Bond, T. C.: Spectral dependence of visible light absorption by carbonaceous particles emitted from coal combustion, Geophys. Res. Lett., 28, 4075-4078, 2001.

Bradsher, K.: Trucks power China's economy, at a suffocating cost.: available at: http://www.nytimes.com/2007/12/08/world/asia/08trucks.html, 2007.

Brooks, B. J., Smith, M. H., Hill, M. K., and O'Dowd, C. D.: Size-differentiated volatility analysis of internally mixed laboratory-generated aerosol, J. Aerosol Sci, 33, 555-579, 2002.

Chan, C. K. and Yao, X.: Air pollution in mega cities in China, Atmos. Environ., 42, 1-42, 2008.

Chen, B., Du, K., Wang, Y., Chen, J., Zhao, J., Wang, K., Zhang, F., and Xu, L.: Emission and transport of carbonaceous aerosols in urbanized coastal areas in China, Aerosol Air Qual. Res., 12, 371-378, 2012.

Chen, Y. and Bond, T. C.: Light absorption by organic carbon from wood combustion, Atmos. Chem. Phys., 10, 1773-1787, 2010.

Cheng, Y., He, K., Duan, F., Zheng, M., Du, Z., Ma, Y., and Tan, J.: Ambient organic carbon to elemental carbon ratios: Influences of the measurement methods and implications, Atmos. Environ., 45, 2060-2066, 2011.

Cheng, Y. F., Eichler, H., Wiedensohler, A., Heintzenberg, J., Zhang, Y. H., Hu, M., Herrmann, H., Zeng, L. M., Liu, S., Gnauk, T., Brüggemann, E., and He, L. Y.: Mixing state of elemental carbon and non-light-absorbing aerosol components derived from in situ particle optical properties at Xinken in Pearl River Delta of China, J. Geophys. Res.-Atmos., 111, D20204, 2006.

Cheng, Y. F., Su, H., Rose, D., Gunthe, S. S., Berghof, M., Wehner, B., Achtert, P., Nowak, A., Takegawa, N., Kondo, Y., Shiraiwa, M., Gong, Y. G., Shao, M., Hu, M., Zhu, T., Zhang, Y. H., Carmichael, G. R., Wiedensohler, A., Andreae, M. O., and Pöschl, U.: Size-resolved measurement of the mixing state of soot in the megacity Beijing, China: diurnal cycle, aging and parameterization, Atmos. Chem. Phys., 12, 4477-4491, 2012.

Chow, J. C., Watson, J. G., Lowenthal, D. H., Solomon, P. A., Magliano, K. L., Ziman, S. D., and Richards, L. W.: PM10 and PM2.5 compositions in California's San Joaquin Valley, Aerosol Sci. Technol., 18, 105-128, 1993.

Chow, J. C., Watson, J. G., Lu, Z., Lowenthal, D. H., Frazier, C. A., Solomon, P. A., Thuillier, R. H., and Magliano, K.: Descriptive analysis of PM2.5 and PM10 at regionally representative locations during SJVAQS/AUSPEX, Atmos. Environ., 30, 2079-2112, 1996.

Chow, J. C., Yu, J. Z., Watson, J. G., Hang Ho, S. S., Bohannan, T. L., Hays, M. D., and Fung, K. K.: The application of thermal methods for determining chemical composition of carbonaceous aerosols: A review, J. Environ. Sci. Heal. A, 42, 1521-1541, 2007.

Donahue, N. M., Robinson, A. L., and Pandis, S. N.: Atmospheric organic particulate matter: From smoke to secondary organic aerosol, Atmos. Environ., 43, 94-106, 2009.

Frey, A., Rose, D., Wehner, B., Müller, T., Cheng, Y., Wiedensohler, A., and Virkkula, A.: Application of the Volatility-TDMA Technique to Determine the Number Size Distribution and Mass Concentration of Less Volatile Particles, Aerosol Sci. Technol., 42, 817-828, 2008.

Fuller, K. A., Malm, W. C., and Kreidenweis, S. M.: Effects of mixing on extinction by carbonaceous particles, J. Geophys. Res.-Atmos., 104, 15941-15954, 1999.

Ghazi, R. and Olfert, J. S.: Coating Mass Dependence of Soot Aggregate Restructuring due to Coatings of Oleic Acid and Dioctyl Sebacate, Aerosol Sci. Technol., 47, 192-200, 2012.

Gnauk, T., Müller, K., van Pinxteren, D., He, L.-Y., Niu, Y., Hu, M., and Herrmann, H.: Size-segregated particulate chemical composition in Xinken, Pearl River Delta, China: OC/EC and organic compounds, Atmos. Environ., 42, 6296-6309, 2008.

Gu, J., Du, S., Han, D., Hou, L., Yi, J., Xu, J., Liu, G., Han, B., Yang, G., and Bai, Z.-P.: Major chemical compositions, possible sources, and mass closure analysis of PM2.5 in Jinan, China, Air Qual. Atmos. Heal., 7, 251-262, 2014.

Häkkinen, S. A. K., Äijälä, M., Lehtipalo, K., Junninen, H., Backman, J., Virkkula, A., Nieminen, T., Vestenius, M., Hakola, H., Ehn, M., Worsnop, D. R., Kulmala, M., Petäjä, T., and Riipinen, I.: Long-term volatility measurements of submicron atmospheric aerosol in Hyytiälä, Finland, Atmos. Chem. Phys., 12, 10771-10786, 2012.

Hansen, A. D. A., Rosen, H., and Novakov, T.: The Aethalometer - An Instrument for the Real-Time Measurement of Optical-Absorption by Aerosol-Particles Sci. Total Environ., 36, 191-196, 1984.

Hitzenberger, R., Jennings, S. G., Larson, S. M., Dillner, A., Cachier, H., Galambos, Z., Rouc, A., and Spain, T. G.: Intercomparison of measurement methods for black carbon aerosols, Atmos. Environ., 33, 2823-2833, 1999.

Horvath, H.: Atmospheric light absorption—A review, Atmos. Environ., 27, 293-317, 1993.

Huffman, J. A., Docherty, K. S., Aiken, A. C., Cubison, M. J., Ulbrich, I. M., DeCarlo, P. F., Sueper, D., Jayne, J. T., Worsnop, D. R., Ziemann, P. J., and Jimenez, J. L.: Chemically-resolved aerosol volatility measurements from two megacity field studies, Atmos. Chem. Phys., 9, 7161-7182, 2009.

Japar, S. M., Brachaczek, W. W., Gorse Jr, R. A., Norbeck, J. M., and Pierson, W. R.: The contribution of elemental carbon to the optical properties of rural atmospheric aerosols, Atmos. Environ., 20, 1281-1289, 1986.

Kalberer, M., Paulsen, D., Sax, M., Steinbacher, M., Dommen, J., Prevot, A. S. H., Fisseha, R., Weingartner, E., Frankevich, V., Zenobi, R., and Baltensperger, U.: Science, 303, 1659, 2004.

Kirchstetter, T. W., Novakov, T., and Hobbs, P. V.: Evidence that the spectral dependence of light absorption by aerosols is affected by organic carbon, J. Geophys. Res.-Atmos., 109, D21208, 2004.

Lavanchy, V. M. H., Gäggeler, H. W., Nyeki, S., and Baltensperger, U.: Elemental carbon (EC) and black carbon (BC) measurements with a thermal method and an aethalometer at the high-alpine research station Jungfraujoch, Atmos. Environ., 33, 2759-2769, 1999.

Lee, B. P., Li, Y. J., Yu, J. Z., Louie, P. K. K., and Chan, C. K.: Physical and chemical characterization of ambient aerosol by HR-ToF-AMS at a suburban site in Hong Kong during springtime 2011, J. Geophys. Res.-Atmos., 118, 8625-8639, 2013.

Levy, M. E., Zhang, R., Zheng, J., Tan, H., Wang, Y., Molina, L. T., Takahama, S., Russell, L. M., and Li, G.: Measurements of submicron aerosols at the California–Mexico border during the Cal–Mex 2010 field campaign, Atmos. Environ., 88, 308-319, 2014.

Liousse, C., Cachier, H., and Jennings, S. G.: Optical and thermal measurements of black carbon aerosol content in different environments: Variation of the specific attenuation cross-section, sigma (σ), Atmos. Environ., 27, 1203-1211, 1993.

Lo, J. C. F., Lau, A. K. H., Fung, J. C. H., and Chen, F.: Investigation of enhanced cross-city transport and trapping of air pollutants by coastal and urban land-sea breeze circulations, J. Geophys. Res.-Atmos., 111, D14104, 2006.

Murphy, B. N., Donahue, N. M., Robinson, A. L., and Pandis, S. N.: A naming convention for atmospheric organic aerosol, Atmos. Chem. Phys., 14, 5825-5839, 2014.

Novakov, T., Ramanathan, V., Hansen, J. E., Kirchstetter, T. W., Sato, M., Sinton, J. E., and Sathaye, J. A.: Large historical changes of fossil-fuel black carbon aerosols, Geophys. Res. Lett., 30, 4, 2003.

Onasch, T. B., Trimborn, A., Fortner, E. C., Jayne, J. T., Kok, G. L., Williams, L. R., Davidovits, P., and Worsnop, D. R.: Soot Particle Aerosol Mass Spectrometer: Development, Validation, and Initial Application, Aerosol Sci. Technol., 46, 804-817, 2012.

Penner, J. E. and Novakov, T.: Carbonaceous particles in the atmosphere: A historical perspective to the Fifth International Conference on Carbonaceous Particles in the Atmosphere, J. Geophys. Res.-Atmos., 101, 19373-19378, 1996.

Petzold, A. and Schönlinner, M.: Multi-angle absorption photometry—a new method for the measurement of aerosol light absorption and atmospheric black carbon, J. Aerosol Sci, 35, 421-441, 2004.

Philippin, S., Wiedensohler, A., and Stratmann, F.: Measurements of non-volatile fractions of pollution aerosols with an eight-tube volatility tandem differential mobility analyzer (VTDMA-8), J. Aerosol Sci, 35, 185-203, 2004.

Pinnick, R., Jennings, S., and Fernandez, G.: Volatility of aerosols in the arid southwestern United States, J. Atmos. Sci., 44, 562-576, 1987.

Putaud, J. P., Van Dingenen, R., Alastuey, A., Bauer, H., Birmili, W., Cyrys, J., Flentje, H., Fuzzi, S., Gehrig, R., Hansson, H. C., Harrison, R. M., Herrmann, H., Hitzenberger, R., Hüglin, C., Jones, A. M., Kasper-Giebl, A., Kiss, G., Kousa, A., Kuhlbusch, T. A. J., Löschau, G., Maenhaut, W., Molnar, A., Moreno, T., Pekkanen, J., Perrino, C., Pitz, M., Puxbaum, H., Querol, X., Rodriguez, S., Salma, I., Schwarz, J., Smolik, J., Schneider, J., Spindler, G., ten Brink, H., Tursic, J., Viana, M., Wiedensohler, A., and Raes, F.: A European aerosol phenomenology – 3: Physical and chemical characteristics of particulate matter from 60 rural, urban, and kerbside sites across Europe, Atmos. Environ., 44, 1308-1320, 2010.

Rader, D. J. and McMurry, P. H.: Application of the tandem differential mobility analyzer to studies of droplet growth or evaporation, J. Aerosol Sci, 17, 771-787, 1986.

Robinson, A. L., Donahue, N. M., Shrivastava, M. K., Weitkamp, E. A., Sage, A. M., Grieshop, A. P., Lane, T. E., Pierce, J. R., and Pandis, S. N.: Rethinking organic aerosols: Semivolatile emissions and photochemical aging, Science, 315, 1259-1262, 2007.

Rolph, G. D.: Real-time Environmental Applications and Display sYstem (READY) Website (http://www.ready.noaa.gov). NOAA Air Resources Laboratory, College Park, MD., 2016.

Rose, D., Wehner, B., Ketzel, M., Engler, C., Voigtländer, J., Tuch, T., and Wiedensohler, A.: Atmospheric number size distributions of soot particles and estimation of emission factors, Atmos. Chem. Phys., 6, 1021-1031, 2006.

Rose, D., Gunthe, S. S., Su, H., Garland, R. M., Yang, H., Berghof, M., Cheng, Y. F., Wehner, B., Achtert, P., Nowak, A., Wiedensohler, A., Takegawa, N., Kondo, Y., Hu, M., Zhang, Y., Andreae, M. O., and Pöschl, U.: Cloud condensation nuclei in polluted air and biomass burning smoke near the mega-city Guangzhou, China – Part 2: Size-resolved aerosol chemical composition, diurnal cycles, and externally mixed weakly CCN-active soot particles, Atmos. Chem. Phys., 11, 2817-2836, 2011.

Rosen, H., Hansen, A. D. A., Gundel, L., and Novakov, T.: Identification of the optically absorbing component in urban aerosols, Appl. Opt., 17, 3859-3861, 1978.

Schauer, J. J., Mader, B. T., Deminter, J. T., Heidemann, G., Bae, M. S., Seinfeld, J. H., Flagan, R. C., Cary, R. A., Smith, D., Huebert, B. J., Bertram, T., Howell, S., Kline, J. T., Quinn, P., Bates, T., Turpin, B., Lim, H. J., Yu, J. Z., Yang, H., and Keywood, M. D.: ACE-Asia intercomparison of a thermal-optical method for the determination of particle-phase organic and elemental carbon, Environ. Sci. Technol., 37, 993-1001, 2003.

Smith, J. N., Dunn, M. J., VanReken, T. M., Iida, K., Stolzenburg, M. R., McMurry, P. H., and Huey, L. G.: Chemical composition of atmospheric nanoparticles formed from nucleation in Tecamac, Mexico: Evidence for an important role for organic species in nanoparticle growth, Geophys. Res. Lett., 35, L04808, 2008.

Stein, A. F., Draxler, R. R., Rolph, G. D., Stunder, B. J. B., Cohen, M. D., and Ngan, F.: NOAA's HYSPLIT Atmospheric Transport and Dispersion Modeling System, B. Am. Meteorol. Soc., 96, 2059-2077, 2015.

Stephens, M., Turner, N., and Sandberg, J.: Particle identification by laser-induced incandescence in a solid-state laser cavity, Appl. Opt., 42, 3726-3736, 2003.

Tan, H. B., Yin, Y., Gu, X. S., Li, F., Chan, P. W., Xu, H. B., Deng, X. J., and Wan, Q. L.: An observational study of the hygroscopic properties of aerosols over the Pearl River Delta region, Atmos. Environ., 77, 817-826, 2013a.

Tan, H. B., Xu, H. B., Wan, Q. L., Li, F., Deng, X. J., Chan, P. W., Xia, D., and Yin, Y.: Design and Application of an Unattended Multifunctional H-TDMA System, J. Atmos. Ocean Tech., 30, 1136-1148, 2013b.

Tao, J., Zhang, L., Ho, K., Zhang, R., Lin, Z., Zhang, Z., Lin, M., Cao, J., Liu, S., and Wang, G.: Impact of PM2.5 chemical compositions on aerosol light scattering in Guangzhou — the largest megacity in South China, Atmos. Res., 135–136, 48-58, 2014.

Turpin, B. J., Cary, R. A., and Huntzicker, J. J.: An In Situ, Time-Resolved Analyzer for Aerosol Organic and Elemental Carbon, Aerosol Sci. Technol., 12, 161-171, 1990.

Twomey, S.: On the composition of cloud nuclei in the northeastern United States, J. Rech. Atmos, 3, 281-285, 1968.

Villani, P., Picard, D., Marchand*, N., and Laj, P.: Design and Validation of a 6-Volatility Tandem Differential Mobility Analyzer (VTDMA), Aerosol Sci. Technol., 41, 898-906, 2007.

Virkkula, A., Ahlquist, N. C., Covert, D. S., Arnott, W. P., Sheridan, P. J., Quinn, P. K., and Coffman, D. J.: Modification, Calibration and a Field Test of an Instrument for Measuring Light Absorption by Particles, Aerosol Sci. Technol., 39, 68-83, 2005.

Wehner, B., Philippin, S., Wiedensohler, A., Scheer, V., and Vogt, R.: Variability of non-volatile fractions of atmospheric aerosol particles with traffic influence, Atmos. Environ., 38, 6081-6090, 2004.

Wehner, B., Berghof, M., Cheng, Y. F., Achtert, P., Birmili, W., Nowak, A., Wiedensohler, A., Garland, R. M., Pöschl, U., Hu, M., and Zhu, T.: Mixing state of nonvolatile aerosol particle fractions and comparison with light absorption in the polluted Beijing region, J. Geophys. Res.-Atmos., 114, D00G17, 2009.

Wu, C., Ng, W. M., Huang, J. X., Wu, D., and Yu, J. Z.: Determination of Elemental and Organic Carbon in PM2.5 in the Pearl River Delta Region: Inter-Instrument (Sunset vs. DRI Model 2001 Thermal/Optical Carbon Analyzer) and Inter-Protocol Comparisons (IMPROVE vs. ACE-Asia Protocol), Aerosol Sci. Technol., 46, 610-621, 2012.

Wu, D., Bi, X. Y., Deng, X. J., Li, F., Tan, H. B., Liao, G. L., and Huang, J.: Effect of atmospheric haze on the deterioration of visibility over the Pearl River Delta, Acta Meteorol. Sin., 21, 215-223, 2007.

Yu, H., Wu, C., Wu, D., and Yu, J. Z.: Size distributions of elemental carbon and its contribution to light extinction in urban and rural locations in the pearl river delta region, China, Atmos. Chem. Phys., 10, 5107-5119, 2010.

Yue, D. L., Zhong, L. J., Zhang, T., J., S., L., Y., Q.., Y. S., Y., Z., and Zeng, L. M.: Particle Growth and Variation of Cloud Condensation Nucleus Activity on Polluted Days with New Particle Formation: A Case Study for Regional Air Pollution in the PRD Region, China, Aerosol Air Qual. Res., 16, 323-335, 2016.

Zhang, Q., Stanier, C. O., Canagaratna, M. R., Jayne, J. T., Worsnop, D. R., Pandis, S. N., and Jimenez, J. L.: Insights into the Chemistry of New Particle Formation and Growth Events in Pittsburgh Based on Aerosol Mass Spectrometry, Environ. Sci. Technol., 38, 4797-4809, 2004.

Zhang, S. L., Ma, N., Kecorius, S., Wang, P. C., Hu, M., Wang, Z. B., Größ, J., Wu, Z. J., and Wiedensohler, A.: Mixing state of atmospheric particles over the North China Plain, Atmos. Environ., 125, Part A, 152-164, 2016.

Zhang, Y., Wang, X., Li, G., Yang, W., Huang, Z., Zhang, Z., Huang, X., Deng, W., Liu, T., Huang, Z., and Zhang, Z.: Emission factors of fine particles, carbonaceous aerosols and traces gases from road vehicles: Recent tests in an urban tunnel in the Pearl River Delta, China, Atmos. Environ., 122, 876-884, 2015.

Zhang, Y. M., Zhang, X. Y., Sun, J. Y., Lin, W. L., Gong, S. L., Shen, X. J., and Yang, S.: Characterization of new particle and secondary aerosol formation during summertime in Beijing, China, Tellus B, 63, 382-394, 2011.

Table 1. Temperature (T) and residence time (RT) protocol of the semi-continuous Sunset OC/EC analyzer (Wu et al., 2012)

Carbon Fraction	Carrier Gas	T (°C)	RT (s)
OC_1	He	310	80
OC_2		475	60
OC_3		615	60
OC_4		870	90
EC_1	He and 2% O_2	550	45
EC_2		625	45
EC_3		700	45
EC_4		775	45
EC_5		850	45
EC_6		870	45

Table 2. Summary of average number and volume fractions in VTDMA measurements at 300°C.

Diameter (nm)	40	80	110	150	200	300
Number fraction						
CV	0.380 ± 0.153	0.174 ± 0.097	0.188 ± 0.081	0.167 ± 0.074	0.153 ± 0.070	0.141 ± 0.065
HV	0.255 ± 0.097	0.198 ± 0.052	0.165 ± 0.055	0.163 ± 0.064	0.178 ± 0.081	0.214 ± 0.097
MV	0.314 ± 0.097	0.513 ± 0.089	0.515 ± 0.098	0.530 ± 0.105	0.523 ± 0.116	0.497 ± 0.125
LV	0.051 ± 0.026	0.113 ± 0.040	0.132 ± 0.041	0.140 ± 0.041	0.146 ± 0.044	0.148 ± 0.047
Volume fraction						
VM	0.503 ± 0.131	0.600 ± 0.082	0.580 ± 0.073	0.590 ± 0.066	0.602 ± 0.064	0.627 ± 0.064
CV	0.361 ± 0.168	0.163 ± 0.105	0.166 ± 0.098	0.148 ± 0.086	0.134 ± 0.080	0.127 ± 0.073
HV	0.014 ± 0.005	0.011 ± 0.003	0.008 ± 0.002	0.007 ± 0.003	0.007 ± 0.003	0.007 ± 0.003
MV	0.070 ± 0.025	0.112 ± 0.024	0.112 ± 0.025	0.115 ± 0.026	0.109 ± 0.027	0.091 ± 0.025
LV	0.052 ± 0.026	0.114 ± 0.040	0.134 ± 0.044	0.140 ± 0.042	0.148 ± 0.048	0.148 ± 0.047

Table 3. Summary of concentrations of $PM_{2.5}$, OC, EC and the ratio of OC to EC (OC/EC) in the five clusters.

	Cluster				
	Coastal	Maritime	Continental		
	1	2	3	4	5
Origin (to the site)	NE	NE/E	NE	NW	NW
$PM_{2.5}$ (μg m^{-3})	58.5 ± 24.4	58.9 ± 30.9	47.5 ± 28.4	33.9 ± 15.9	33.8 ± 19.3
OC (μg m^{-3})	10.8 ± 6.01	10.84 ± 7.22	10.13 ± 6.89	5.51 ± 3.3	7.32 ± 2.75
EC (μg m^{-3})	4.38 ± 2.97	4.98 ± 4.21	3.43 ± 3.12	1.8 ± 0.98	2.46 ± 0.59
OC/EC	2.83 ± 1.05	2.62 ± 1.03	3.65 ± 1.6	3.18 ± 1.26	2.94 ± 0.73

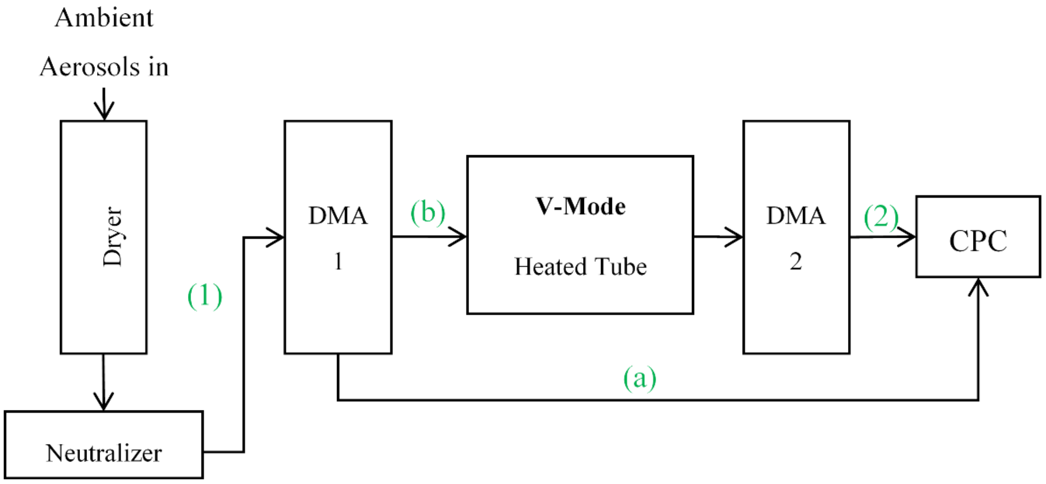

Fig. 1. A Schematic diagram of the volatility tandem differential mobility analyzer (VTDMA).

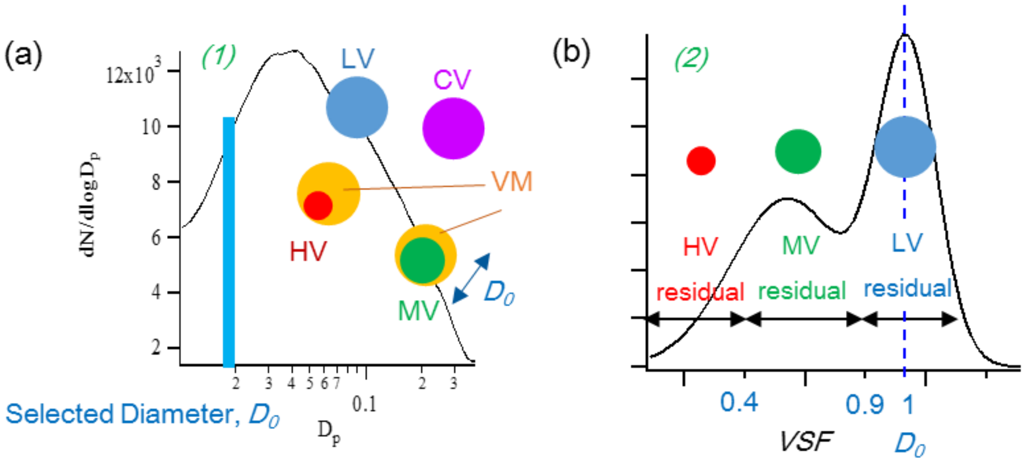

Fig. 2. Examples of particle size distributions of (a) ambient aerosols before entering DMA$_1$ and (b) residuals of the size-selected particles (D_0) after heating. at 300°C. The distributions in Fig. 2a and 2b correspond to (1) and (2) in Figure 1 respectively. Residuals are divided into three groups—LV (blue), MV (green) and HV (red)—based on their *VSF*. CV (purple) and VM (orange) are vaporized and hence not measured as residuals. VM appears as coating for illustration purposes only. It does not necessarily reflect the morphology of the particles.

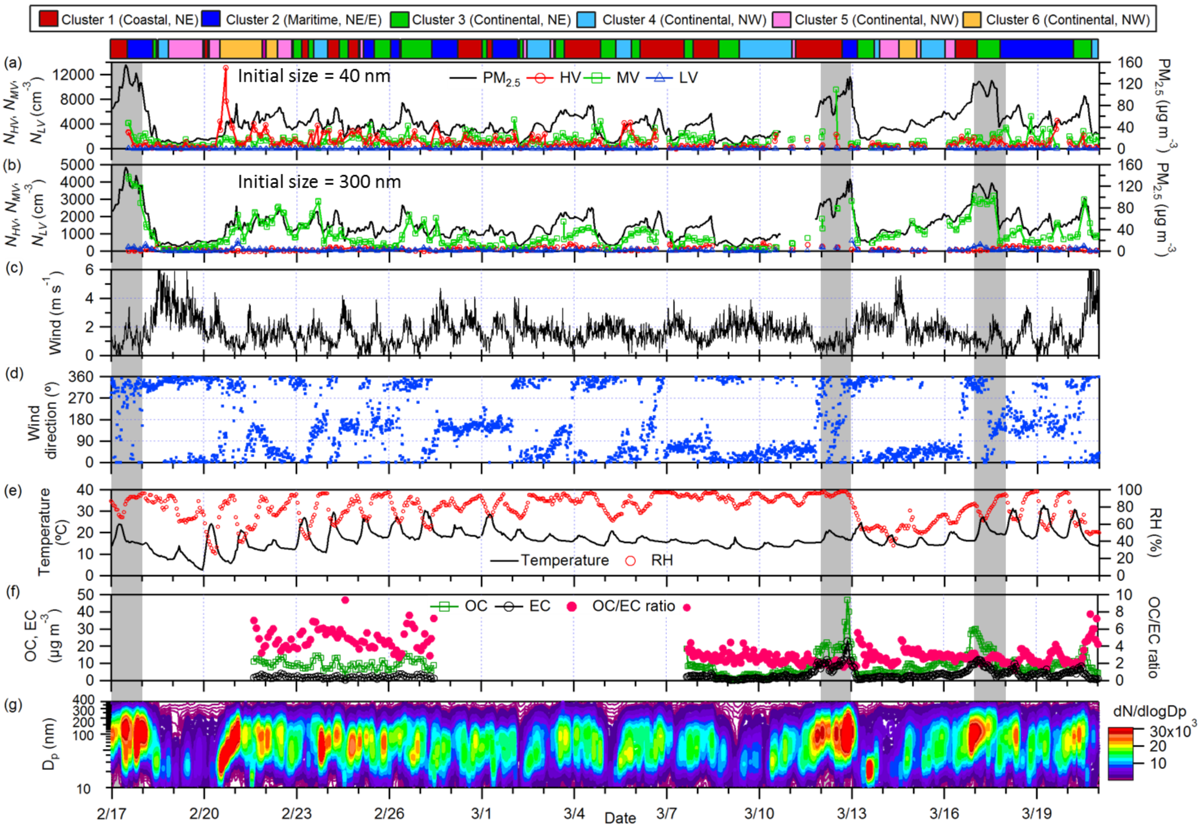

Fig. 3. Temporal variation of number concentrations of HV, MV and LV in 40 nm and 300 nm particles, $PM_{2.5}$, major meteorological parameters, OC and EC concentrations, OC-to-EC ratio and particle number size distributions in the campaign. Air mass clusters are depicted at the top and the shaded areas indicate days with daily-averaged $PM_{2.5}$ concentrations exceeding 95 μg m^{-3}.

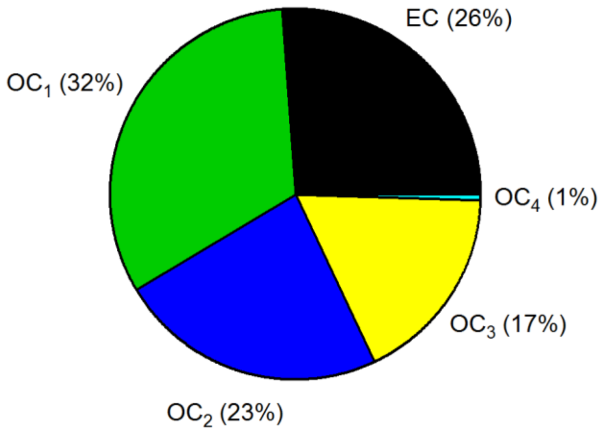

Fig. 4. Average mass fractions of EC, OC_1, OC_2, OC_3 and OC_4 in $PM_{2.5}$.

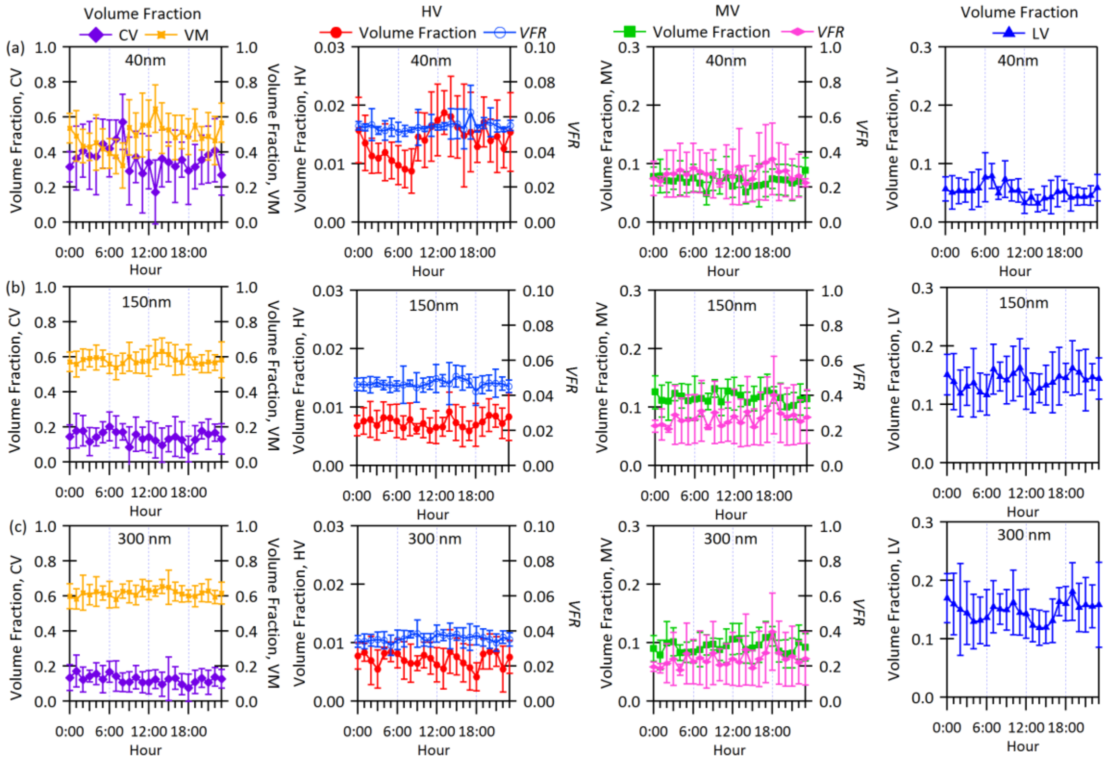

Fig. 5. Diurnal variations in the volume fractions of (columns from left to right) CV, VM, HV residuals, MV residuals and LV residuals in (a) 40 nm, (b) 150 nm and (c) 300 nm particles in February and March 2014. Diurnal variations in the volume fraction remaining (*VFR*) of HV and MV particles are plotted on the right axis. Error bars represent one standard deviation.

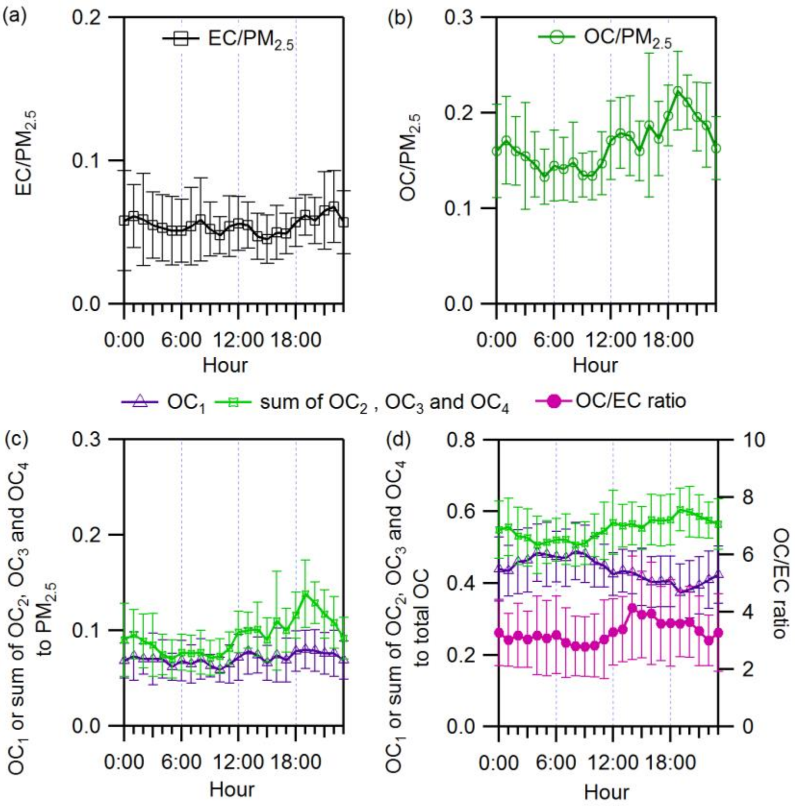

Fig. 6. Diurnal variations in the mass fractions of EC, OC, OC_1 and the sum of OC_2, OC_3 and OC_4 in $PM_{2.5}$, the ratio of OC to EC, mass fractions of OC_1 and the sum of OC_2, OC_3 and OC_4 to total OC in February and March 2014. Error bars represent one standard deviation.

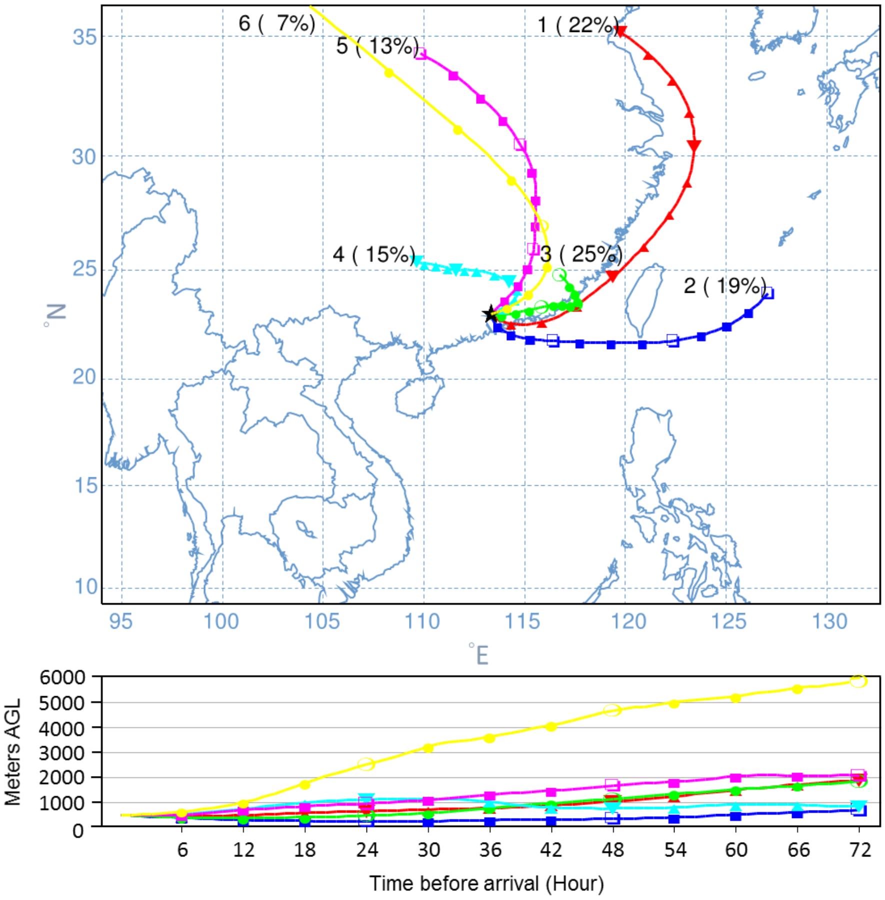

Fig. 7. Mean back trajectories of the six types of air masses arriving at the sampling site.

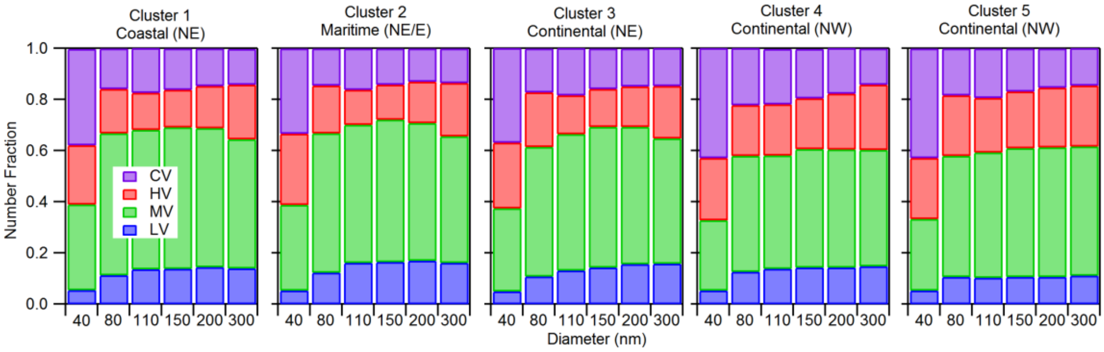

Fig. 8. Average number fractions of CV, HV, MV and LV in clusters 1 to 5 at different selected diameters.

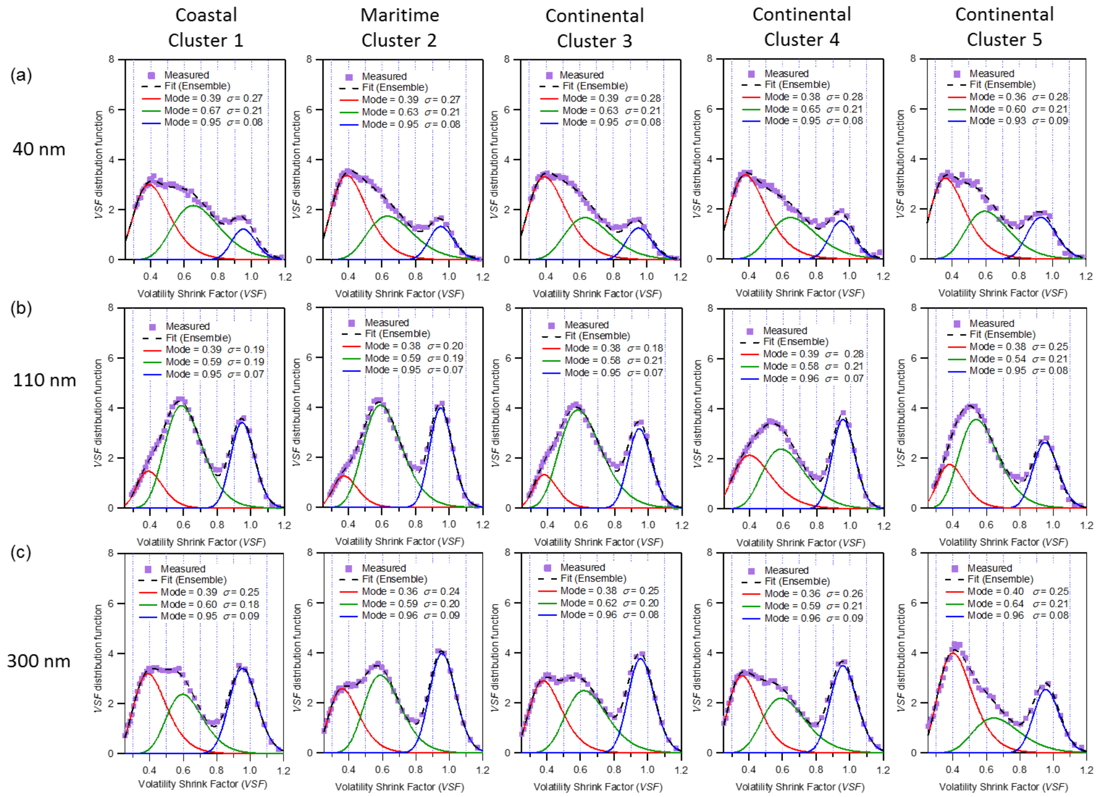

Fig. 9. Volatility shrink factor (*VSF*) distribution function in different clusters. Solid and dotted lines are the peaks fitted with log-normal function and the ensemble distributions, respectively.

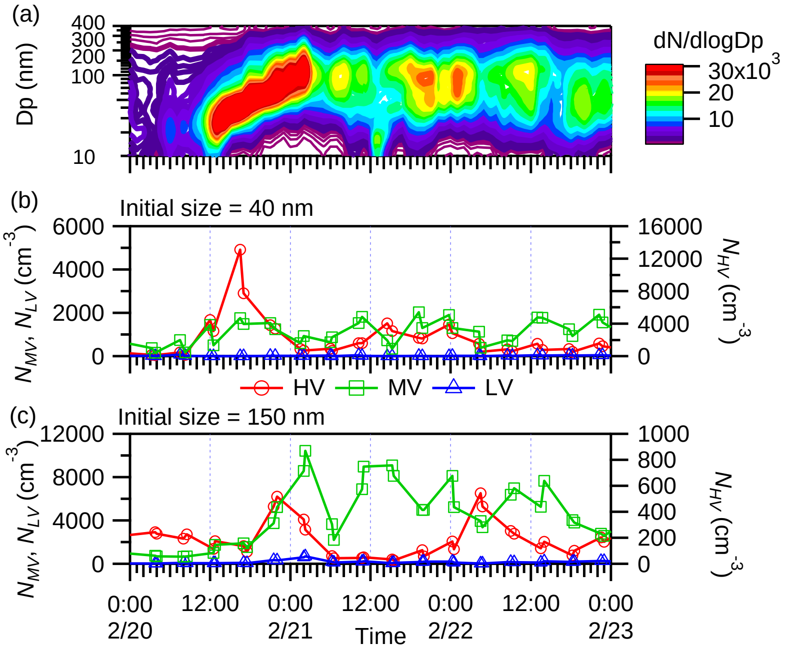

Fig. 10. Time series of (a) particle number size distribution, (b) number concentrations of HV, MV and LV in 40 nm particles and (c) number concentrations of HV, MV and LV in 150 nm particles during a new particle event day on 20 Feb 2014.

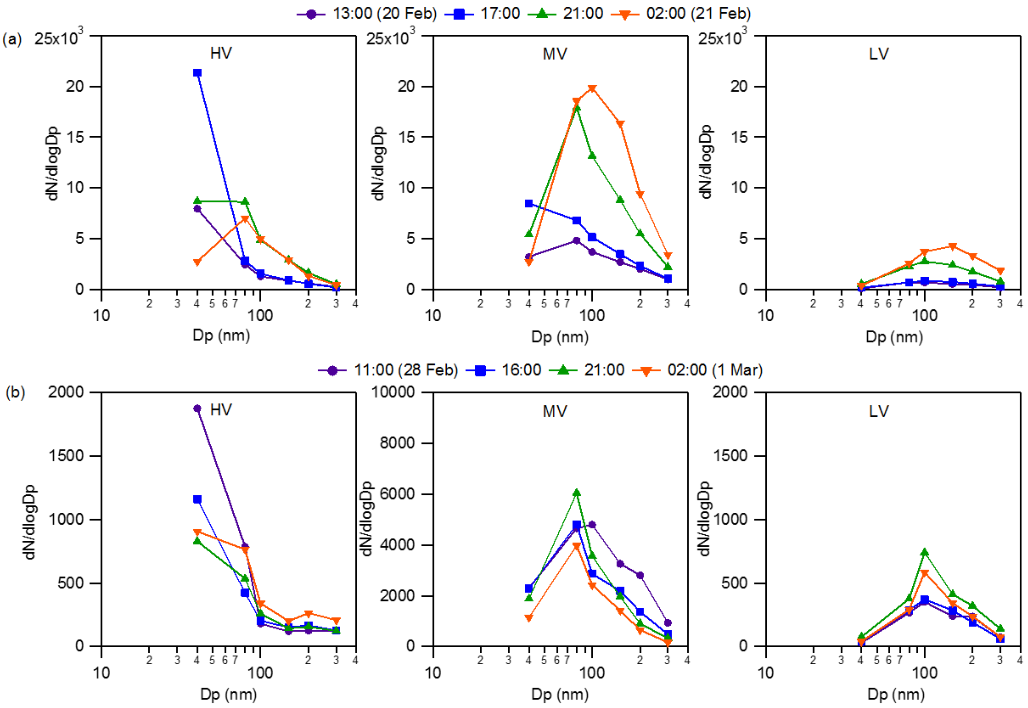

Fig. 11. Particle number size distribution of (columns from left to right) HV, MV and LV particles (a) during a new particle formation event at 13:00, 17:00, 21:00 on 20 Feb and 02:00 on 21 Feb 2014 and (b) during non-event days at 11:00, 16:00, 21:00 on 28 Feb and 02:00 on 1 Mar 2014.

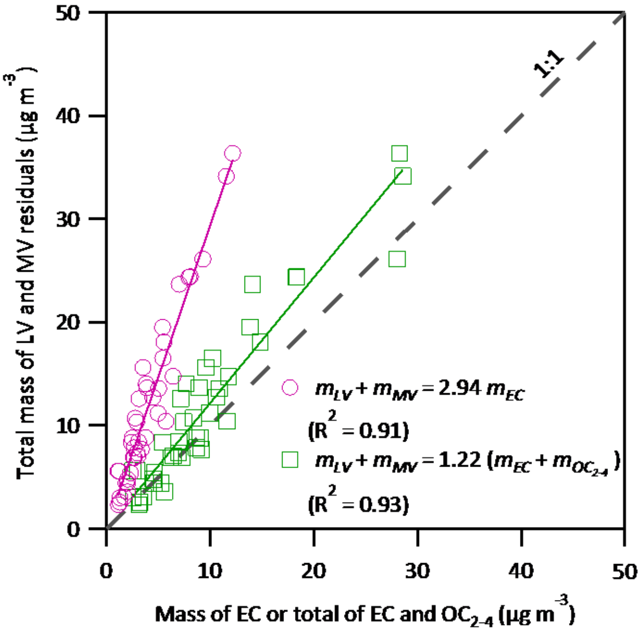

Fig. 12. A closure analysis of the total mass of LV and MV residuals from VTDMA at 300°C and measured mass of EC or total of EC and OC_{2-4} from the OC/EC analyzer.